

Pilot Allocation Based on Simulated Annealing for Sparse Channel Estimation in UWB OFDM Systems

Taoyong Li^{*†}, Nele Noels^{*} and Heidi Steendam^{*}

^{*}Telecommunications and Information Processing Department, Ghent University/IMEC, Gent, Belgium

[†]Collaborative Innovation Center of Information Sensing and Understanding, Xi'an, Shaanxi, China

Email: {Taoyong.Li, Nele.Noels, Heidi.Steendam}@ugent.be

Abstract—In ultra wideband (UWB) orthogonal frequency-division multiplexing (OFDM) systems, compressive sensing (CS) is often employed to produce a pilot-assisted estimate of the sparse channel. The corresponding estimation performance depends to a large extent on the considered pilot allocation (PA) method, i.e., the way to select which OFDM subcarriers are best used to transmit the pilot symbols. The development of good practical PA methods has recently received a lot of attention in the scientific literature. The main challenge is to provide an attractive trade-off between the complexity of the PA method and the achieved channel estimation performance (and by extension the achieved bit error rate). In this paper, we propose a novel PA method based on simulated annealing (SA). Simulations are conducted to confirm the validity of our approach. Compared to the state-of-the-art method, the proposed PA method is shown to achieve better performance with a lower complexity.

Index Terms—Sparse channel estimation, mutual coherence, simulated annealing, pilot allocation, ultra wideband, OFDM, compressive sensing.

I. INTRODUCTION

Orthogonal frequency-division multiplexing (OFDM) is considered as one of the most promising techniques for ultra wideband (UWB) transmission [1]. One of the prerequisites for reliable communication is the availability of accurate channel state information. Hence, the channel needs to be estimated accurately. In this context, we first note that in UWB systems, the sampling period is usually much smaller than the channel delay spread. Hence, the channel will be spread out over many channel taps. However, measurements of the indoor channel show that the channel impulse response (CIR) only contains a limited number of non-zero contributions, i.e., the channel can be modelled as sparse. For example, [2], [3] demonstrate that indoor channel models considered for the IEEE 802.15.4a standard are sparse. In that case, it is attractive to use channel estimation methods that are based on compressive sensing (CS) [4], [5] because this can decrease the overhead in terms of the required amount of pilot subcarriers [2], [3], [6]–[8].

According to the CS theory, a sparse vector can be recovered accurately from a small number of linear measurements. The performance of this procedure is determined by the compressive sensing measurement matrix, i.e., the matrix that

specifies the linear transformation between the measurements and the vector of interest. In [9], it was shown that a small measurement matrix mutual coherence (MMMC) is desirable. This is confirmed by the results presented in [10]–[12], where it was shown that pilot allocation (PA) methods that succeed in decreasing the MMMC, indeed result in an improved channel estimation performance. In [10], the authors propose a random search method. A test set Ω of N_{rest} PAs is randomly selected from the complete set of all N_{total} possible PAs, after which the PA in Ω yielding the smallest MMMC is selected. In general, the performance/complexity trade-off of this method is rather poor. In [11], a low complexity greedy method is proposed to find a good PA. This method has a very low complexity, but yields a MMMC that is far from minimum. In [12], an iterative stochastic sequential search (SSS) algorithm is employed and shown to outperform the methods from [10] and [11] when taking into account both performance and complexity.

In this paper, we investigate the use of simulated annealing (SA) to find a PA with a low MMMC. SA is a well-known technique to solve combinatorial optimization problems. In the past, it has been successfully applied to CS based radar beamforming [13] and resource allocation [14]. In this paper, we show that the proposed method outperforms state-of-the-art SSS method on both performance and complexity.

The rest of the paper is organized as follows. In Section II, we introduce the concept of CS based pilot-assisted channel estimation. The proposed PA method is fully described in Section III. Section IV presents the numerical results. Final conclusions are drawn in Section V.

II. MUTUAL COHERENCE OF THE MEASUREMENT MATRIX

Assume that a cyclic prefix OFDM system consists of N subcarriers. Among these, N_p subcarriers are allocated for frequency-domain pilot-assisted channel estimation. The indices of the pilot subcarriers constitute the PA vector $\mathbf{P} = [p_1, p_2, \dots, p_{N_p}]$. The corresponding pilot symbols are grouped into the vector $\mathbf{X} = [X(p_1), X(p_2), \dots, X(p_{N_p})]$. The OFDM signal is transmitted over a channel with the CIR

$\mathbf{h} = [h(0), h(1), \dots, h(L-1)]^T$ of length L . The CIR \mathbf{h} is sparse, meaning that only $K \ll L$ taps $h(k)$ of \mathbf{h} have significant values while all the other taps are (almost) zero. We will further assume that the length of the cyclic prefix exceeds the channel duration L and we will restrict our attention to the observation of the pilot subcarriers. After cyclic prefix removal and discrete Fourier transform (DFT) operation, we obtain the observation vector $\mathbf{Y} = [Y(p_1), Y(p_2), \dots, Y(p_{N_p})]^T$:

$$\mathbf{Y} = \text{diag}(\mathbf{X})\mathbf{F}_{N_p \times L}\mathbf{h} + \mathbf{N}_e, \quad (1)$$

where $\mathbf{N}_e = [N_e(p_1), N_e(p_2), \dots, N_e(p_{N_p})]^T \sim \mathcal{CN}(\mathbf{0}, \sigma^2\mathbf{I}_{N_p})$ is additive white Gaussian noise, and $\mathbf{F}_{N_p \times L}$ is the DFT submatrix, given by

$$\mathbf{F}_{N_p \times L} = \frac{1}{\sqrt{N}} \begin{bmatrix} 1 & \omega^{p_1} & \dots & \omega^{p_1 \cdot (L-1)} \\ 1 & \omega^{p_2} & \dots & \omega^{p_2 \cdot (L-1)} \\ \vdots & \vdots & \ddots & \vdots \\ 1 & \omega^{p_{N_p}} & \dots & \omega^{p_{N_p} \cdot (L-1)} \end{bmatrix}, \quad (2)$$

where $\omega = e^{-j2\pi/N}$, and N is the DFT size. Let $\Phi = \text{diag}(\mathbf{X})\mathbf{F}_{N_p \times L}$, then (1) can be rewritten as

$$\mathbf{Y} = \Phi\mathbf{h} + \mathbf{N}_e. \quad (3)$$

The CIR \mathbf{h} can be estimated accurately from (3) by means of a conventional method like the least-square (LS) method provided that $N_p \geq L$ [15]. However, if the CIR \mathbf{h} is sparse, CS theory can be applied to estimate \mathbf{h} from (3) with $N_p < L$, which is advantageous in terms of power and bandwidth efficiency. In the latter case, an estimate $\hat{\mathbf{h}}$ is found, e.g., through solving the following popular convex l_1 -norm optimization problem [4]:

$$\hat{\mathbf{h}} = \min\|\mathbf{h}\|_1 \quad \text{s.t.} \quad \mathbf{Y} = \Phi\mathbf{h}, \quad (4)$$

where Φ is called the measurement matrix. From [9]–[12], it follows that a smaller MMMC results in a more accurate estimate $\hat{\mathbf{h}}$ of \mathbf{h} . The mutual coherence of Φ is defined as:

$$\begin{aligned} \mu\{\Phi\} &= \max_{1 \leq m < n \leq L} \frac{|\langle \Phi_{\mathbf{m}}, \Phi_{\mathbf{n}} \rangle|}{\|\Phi_{\mathbf{m}}\|_2 \|\Phi_{\mathbf{n}}\|_2}, \\ &= \max_{1 \leq m < n \leq L} \left| \frac{\sum_{i=1}^{N_p} |X(p_i)|^2 \omega^{p_i(n-m)}}{\sum_{j=1}^{N_p} |X(p_j)|^2} \right|, \end{aligned} \quad (5)$$

where $\Phi_{\mathbf{m}}$ and $\Phi_{\mathbf{n}}$ respectively denote the m -th and the n -th columns of Φ , $\langle \cdot \rangle$ represents the scalar product operation, $\|\cdot\|_2$ is the l_2 -norm, and $|X(p_i)|^2$ stands for the power of the i -th pilot symbol. In the special case where all pilot symbols have the same power, i.e.,

$$|X(p_1)|^2 = |X(p_2)|^2 = \dots = |X(p_{N_p})|^2 = P_{\text{pilot}}, \quad (6)$$

(5) reduces to:

$$\mu\{\Phi\} = \max_{1 \leq m < n \leq L} \left| \sum_{i=1}^{N_p} \frac{1}{N_p} \omega^{p_i(n-m)} \right|. \quad (7)$$

The existing PA methods from [10]–[12] are all attempts to find, in an efficient way, a PA vector \mathbf{P} that yields a value of $\mu\{\Phi\}$ that is close to minimum.

III. PILOT ALLOCATION METHOD BASED ON SIMULATED ANNEALING ALGORITHM

Finding the PA that minimizes the MMMC $\mu\{\Phi\}$ can be described by the following combinatorial optimization problem:

$$\min_{\mathbf{P}} \mu\{\Phi\} \quad \text{s.t.} \quad \mathbf{P} \subset \Xi, \quad (8)$$

with $\Xi = \{1, 2, \dots, N\}$. A well-known heuristic algorithm to approximately solve combinatorial optimization problems with an acceptable accuracy and in a reasonable time is SA [16]. In Algorithm 1, we show how SA can be applied to solve (8). In this algorithm, we randomly change the position p_k of a pilot symbol, and compute the MMMC $\mu\{\Phi\}_{\text{temp}}$ for the new PA. If $\mu\{\Phi\}_{\text{temp}}$ of the new PA is better than the MMMC $\mu\{\Phi\}$ of the old PA, i.e., $\mu\{\Phi\}_{\text{temp}} - \mu\{\Phi\} < 0$, we update the PA. However, if we just change one pilot symbol at the same time, using only this condition is equivalent to searching for an optimum in the neighborhood of the initial PA, implying we risk to get stuck in a local optimum. To solve this issue, SA allows a new PA to be selected, even if the MMMC is not better than the old PA. This is done by adding the condition

$$\exp\left(\frac{-(\mu\{\Phi\}_{\text{temp}} - \mu\{\Phi\})}{T}\right) > \text{rand}(), \quad (9)$$

i.e., the new PA is selected, even when $\mu\{\Phi\}_{\text{temp}} - \mu\{\Phi\} > 0$, if the exponential of (9) is larger than a random value generated with a continuous uniform distribution from 0 to 1, i.e., $\text{rand}() \sim U[0, 1]$. The exponential in (9) depends on the parameter T , which is called the temperature of the SA algorithm. If T is large, the probability that the condition (9) is fulfilled is large, implying the algorithm can easily escape a local optimum. However, for large T , this easiness to escape an optimum also hinders the convergence if we are close to the global optimum, as the probability that the algorithm jumps away from the global optimum is large. Therefore, in the SA algorithm, we start with a high initial temperature, T_{init} , and gradually reduce the temperature by scaling the temperature with $T_{\text{rate}} < 1$, and end the algorithm when the temperature reaches a (low) stop temperature T_{stop} (outer loop). For each value of T , the algorithm tries to converge to an optimum by randomly selecting T_{iter} new pilot symbol positions p_k , and checking one by one if at least one of the conditions in line 9 of the algorithm is satisfied (inner loop). The selection of the four parameters of the algorithm can be done following the systematic procedure proposed in [17]. The algorithm randomly selects the pilots to be exchanged. Hence, we need to evaluate the risk of repetition, i.e., that the algorithm starts in a PA, follows some 'path', returns in the initial PA, and keeps following the same loop. However, note that if the total number of subcarriers N and the number of pilot subcarriers N_p are equal to 256 and 32, respectively, the probability of repeated testing is in order of $\frac{1}{N_p(N-N_p)} = 1.4 \cdot 10^{-4}$, indicating the probability of repetition is low, unless the number of subcarriers and the number of pilot subcarriers are very small.

We will evaluate the computational complexity and resulting MMMC in Section IV-A. This computational complexity and achieved final $\mu\{\Phi\}$ both depend on the choice of the initial PA vector and on the value of the 4 design parameters: T_{init} , T_{stop} , T_{rate} and T_{iter} . The computational complexity is dominated by the MMMC calculations involved in Algorithm 1 (line 8). Expressed in terms of the number of complex multiplications (NCM), the evaluation of a single MMMC has complexity $N_p(L-1)$. The number of MMMC calculations performed in Algorithm 1 is $T_{iter} \lceil \log_{T_{rate}} \left(\frac{T_{stop}}{T} \right) \rceil$. This results in a total complexity number of

$$T_{iter} \lceil \log_{T_{rate}} \left(\frac{T_{stop}}{T} \right) \rceil * N_p(L-1). \quad (10)$$

By means of comparison, we also consider the complexity of the state-of-the-art method SSS from [12]. In SSS, $T_{iter,SSS}$ search iterations are performed. During each iteration, every element of the PA vector \mathbf{P} is sequentially updated. The procedure involves $T_{iter,SSS} N_p(N-N_p)$ MMMC calculations. So the total complexity of SSS is

$$N_p(N-N_p) T_{iter,SSS} * N_p(L-1). \quad (11)$$

Algorithm 1 SA-based PA

- 1: Initialization: Set N , N_p , L , T_{init} , T_{stop} , T_{rate} and T_{iter} .
 - 2: Select an initial PA vector $\mathbf{P} = \mathbf{P}_{init}$ and calculate $\mu\{\Phi\}$.
 - 3: Set $T = T_{init}$.
 - 4: **while** $T > T_{stop}$ **do** % outer loop
 - 5: **for** $l = 1 : T_{iter}$ **do** % inner loop
 - 6: Randomly choose an element p_k of \mathbf{P} , $k \in \{1, 2, \dots, N_p\}$;
 - 7: Exchange p_k with a subcarrier position randomly selected from $\Xi \setminus \mathbf{P}$ to form the new PA vector \mathbf{P}_{temp} ;
 - 8: Calculate $\mu\{\Phi\}_{temp}$ with \mathbf{P}_{temp} ;
 - 9: **if** $\mu\{\Phi\}_{temp} - \mu\{\Phi\} < 0$ or $exp(-(\mu\{\Phi\}_{temp} - \mu\{\Phi\})/T) > rand()$ **then**
 - 10: $\mathbf{P} \leftarrow \mathbf{P}_{temp}$;
 - 11: **end if**
 - 12: **end for**
 - 13: $T \leftarrow T * T_{rate}$;
 - 14: **end while**
 - 15: Output \mathbf{P} .
-

IV. NUMERICAL RESULTS

In this section, numerical results are presented. We analyze the performance and the computational complexity of the proposed PA method and we compare the results to those of the state-of-the-art SSS method. In our experiments, a quadrature phase-shift keying modulation (QPSK) OFDM system is adopted, so (7) applies. Unless specified otherwise, the number of subcarriers, the number of pilot subcarriers, the length of the CIR, the number of non-zero CIR taps, the SA parameter values and the number of SSS iterations are set to the values shown in Table I. The CIR \mathbf{h} is modelled with $L = 64$ taps, of

TABLE I
THE SYSTEM SETTING

parameter	value
N	256
N_p	32
L	64
K	12
T_{init}	10^{-1}
T_{stop}	10^{-6}
T_{rate}	0.95
T_{iter}	50
$T_{iter,SSS}$	5

which $K = 12$ non-zero taps are randomly placed. The values of the non-zero taps are independently generated according to a complex Gaussian distribution with mean 0 and variance 1, i.e., $CN(0, 1)$. Compressive sampling matching pursuit (CoSaMP) [18] is adopted as the reconstruction algorithm to estimate the CIR \mathbf{h} . A zero forcing equalizer is used in the receiver.

A. Impact of SA parameters values

As already indicated in Section III, the choice of the SA parameter values affects the complexity and the final $\mu\{\Phi\}$. Here, we evaluate the NCM and the MMMC $\mu\{\Phi\}$ of the proposed method for different settings of T_{init} , T_{stop} , T_{rate} and T_{iter} with $\mathbf{P}_{init} = [1, 9, 17, \dots, 249]$. A test set of 11 different parameter settings, denoted 1 to 11, is considered. The parameter settings and resulting values of the NCM and $\mu\{\Phi\}$ are presented in Table II. Setting 1 adopts the values of T_{init} , T_{stop} , T_{rate} and T_{iter} that will be used throughout the remainder of our analysis. Compared to setting 1, setting 2 (3) has a 10 times lower (higher) value of T_{init} , setting 4 (5) has a 10 times higher (lower) value of T_{stop} , setting 6 (7) has lower (higher) value of T_{rate} and setting 8 (9) has a lower (higher) value of T_{iter} . Table II shows that if T_{init} , T_{rate} or T_{iter} is decreased (increased), the NCM also decreases (increases), while the MMMC increases (decreases). On the contrary, if T_{stop} is increased (decreased), the NCM decreases (increases) while the MMMC increases (decreases). Setting 10 combines the SA parameter values that decrease the NCM and setting 11 combines the SA parameter values that decrease $\mu\{\Phi\}$.

Fig. 1 shows the (NCM, MMMC) value pairs for Settings 1 to 11. As can be observed from the figure, the value of $\mu\{\Phi\}$ can be decreased at the price of a complexity increase. However, we see that the decrease of MMMC slows down significantly for values of NCM larger than that of Setting 1. We conclude that Setting 1 provides a good trade-off between complexity and performance: a property that is key with a view to the practical implementation of the technique.

B. Performance of SA as compared to SSS

We now compare the performance of the proposed PA method, further simply denoted as SA, with SSS. For a fair and relevant comparison, the SA parameters are selected as in Setting 1 (see above) and the SSS parameter $T_{iter,SSS}$ is set to 5. The latter is selected such because our experiments

TABLE II
IMPACT OF SA PARAMETER VALUES

	Setting	T_{init}	T_{stop}	T_{rate}	T_{iter}	NCM	$\mu\{\Phi\}$
T_{init}	1	10^{-1}	10^{-6}	0.95	50	22680000	0.1868
	2	10^{-2}	10^{-6}	0.95	50	18144000	0.1988
	3	1	10^{-6}	0.95	50	27216000	0.1859
T_{stop}	4	10^{-1}	10^{-5}	0.95	50	18144000	0.2025
	5	10^{-1}	10^{-7}	0.95	50	27216000	0.1866
T_{rate}	6	10^{-1}	10^{-6}	0.90	50	11088000	0.2091
	7	10^{-1}	10^{-6}	0.97	50	45763200	0.1845
T_{iter}	8	10^{-1}	10^{-6}	0.95	20	9072000	0.2175
	9	10^{-1}	10^{-6}	0.95	70	38102400	0.1853
lowest NCM combination	10	10^{-2}	10^{-5}	0.90	20	2661120	0.2489
lowest MMMC combination	11	1	10^{-7}	0.97	70	74793600	0.1834

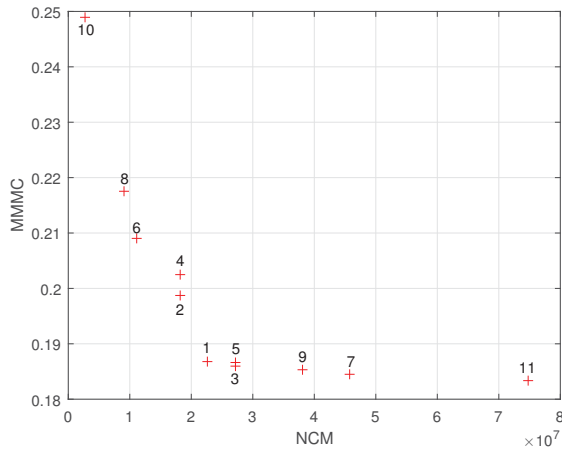


Fig. 1. NCM and MMMC.

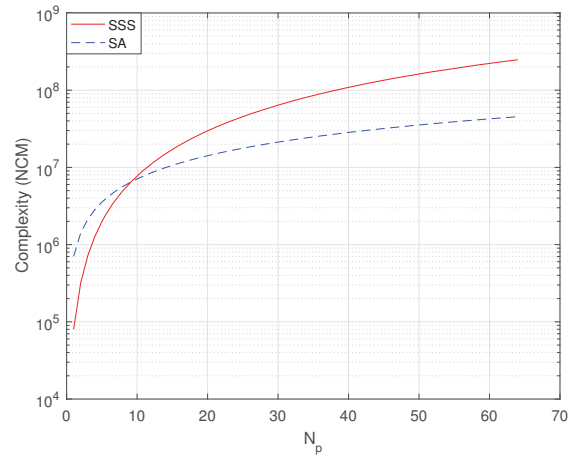


Fig. 2. Complexity comparisons of SA and SSS.

(not shown here) indicate that the MMMC value achieved with SSS converges after about 5 iterations.

We first compare SA and SSS in terms of computational complexity. Fig. 2 shows the numerical NCM values of the two methods as a function of the number of pilot subcarriers. As can be observed in the figure, SA results in a lower complexity than SSS as soon as N_p is larger than 10. Moreover, the complexity advantage of SA as compared to SSS increases significantly as N_p increases beyond $N_p = 10$. The main reason for this is that the complexity of SSS increases proportional to $N_p * N$, while the complexity of SA increases only proportional to $N_p * L$. Comparing the curves in Fig. 2 for $N_p = 64$, we find that the ratio between the NCM of SSS and SA equals 5.4613, which is slightly larger than the predicted $N/L = 4$, valid for large N_p and L , but this difference can easily be explained by evaluating the prefactors of (10) and (11). However, it is clear that the predicted and real ratio are of the same order of magnitude.

To compare SA and SSS in terms of the achieved MMMC, we consider four cases for N_p : $N_p = 26, 28, 30$ and 32 . Table III demonstrates that SA achieves a lower MMMC than SSS in all four cases. In the following we show that this directly translates into a lower normalized mean squared

TABLE III
MMMC WITH SA AND SSS, FOR DIFFERENT VALUES OF N_p

N_p	SA	SSS
26	0.2240	0.2548
28	0.2167	0.2354
30	0.2000	0.2190
32	0.1868	0.1974

channel estimation (NMSE) and a lower bit error rate (BER) for SA than for SSS. To obtain the NMSE and BER, we will have to run the proposed algorithm for different channel realizations and average over these channel realizations. To evaluate how many channel realizations are required to obtain satisfactory results, we show in Fig. 3 the average NMSE for 200, 500, 1000 and 2000 channel realizations, for SA and $N_p = 32$. As can be observed, when the number of channel realizations is at least 500, the curves are indistinguishable, while for 200 realizations, the curve slightly deviates. As the simulation time linearly increases with the number of channel realizations, we therefore set in the remainder of the paper the number of channel realizations equal to 500.

The NMSE of four cases is evaluated by means of a Monte Carlo computer simulation. As a benchmark, we also consider

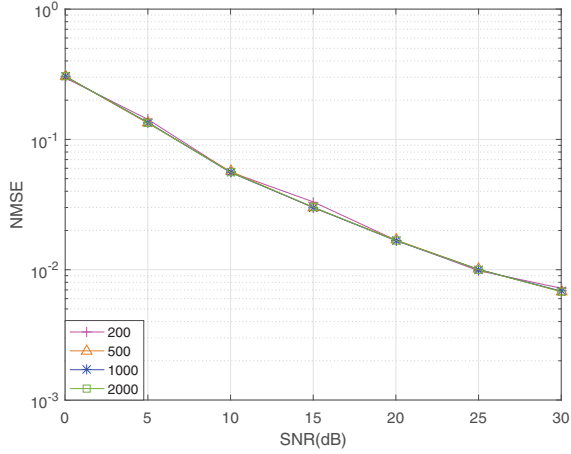
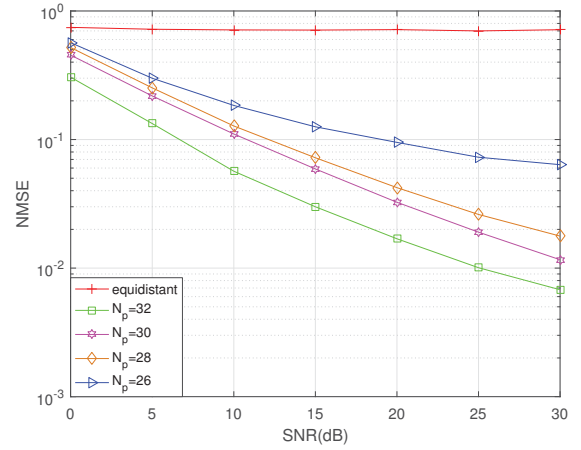


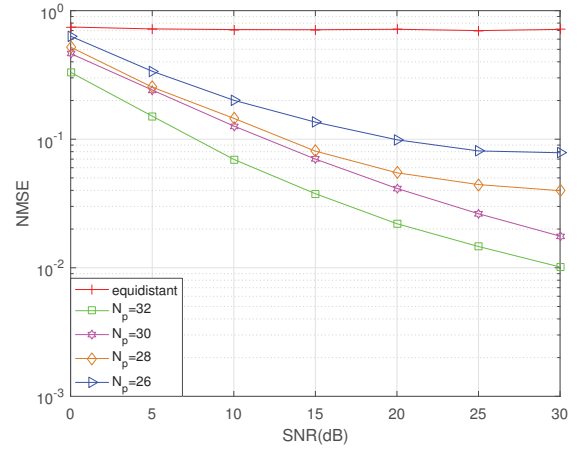
Fig. 3. Monte Carlo experiments for SA with $N_p = 32$.

the NMSE that is obtained with the equidistant PA vector $\mathbf{P}_{equi} = [1, 9, 17, \dots, 249]$ with $N_p = 32$ and where $p_{i+1} - p_i$ is fixed and equal to $N/N_p = 8$. The MMMC corresponding to \mathbf{P}_{equi} is 1 (see (7)), which is the maximum possible value for $\mu\{\Phi\}$ [19]. Fig. 4 shows that, although the number of pilot subcarriers of the equidistant PA is larger than (or equal to) that of the PAs designed by SA or SSS, the channel estimation performance with the equidistant PA is really poor. We observe that the NMSE of SSS and SA improves if the number of pilot subcarriers increases. Moreover, for a given value of N_p , SA results in a lower NMSE than SSS. This is in correspondence with the tendency of the MMMC results presented in Table III. To demonstrate that the proposed PA technique not only outperforms the state-of-the-art technique SSS when combined with CoSaMP, we also combined the two PA techniques with other CS techniques, i.e., subspace pursuit (SP) [20] and orthogonal matching pursuit (OMP) [21]. The NMSE for the different combinations is shown in Fig. 5. From the figure, it follows that the NMSE is essentially independent of the used CS technique, and that the proposed PA technique, SA, clearly outperforms SSS. Note that SP and OMP have a higher computational complexity than CoSaMP.

To evaluate the BER performance, we simulate 500 frames of 5000 OFDM symbols each, whereby we assume that the channel remains fixed over the duration of a frame but varies from frame to frame. The results are presented in Fig. 6 as a function of the SNR P_{pilot}/N_0 . Due to the inaccurate channel estimate results, the BER in the case of the equidistant PA is really large. The BER performance can be significantly improved by applying PAs designed by SSS or SA. In particular, thanks to the lower MMMC, SA achieves a better BER performance than SSS. Furthermore, the results in the figure also show that the use of SA can effectively improve the transmission efficiency: for a given SNR, a smaller amount of pilot subcarriers is required with SA to achieve a given value of the BER than with SSS.



(a)



(b)

Fig. 4. NMSE Performance comparisons of different N_p : (a) SA (b) SSS

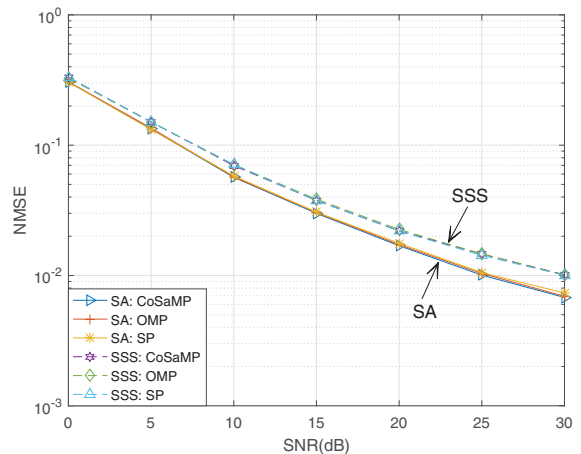


Fig. 5. NMSE performance comparisons of SP, OMP and CoSaMP for SA and SSS with $N_p = 32$.

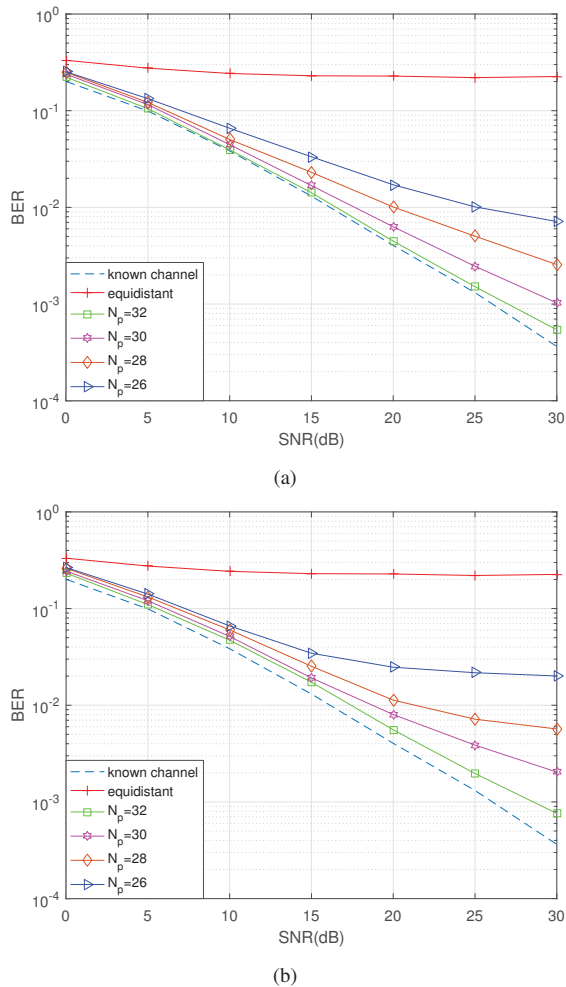


Fig. 6. BER Performance comparisons of different N_p : (a) SA (b) SSS

V. CONCLUSION

UWB communication channels can often be modelled as sparse so that CS techniques can be applied for channel estimation. The performance of CS based sparse channel estimation can be improved by decreasing a quantity referred to as the MMMC. In this paper, we propose a novel PA method that minimizes the MMMC via SA. Compared to the state-of-the-art PA method, the proposed method is shown to obtain a lower MMMC with a lower complexity, and by extension a more accurate channel estimation and thus a better BER performance. The numerical results indicate that an equidistant PA is not recommended in CS based pilot-assisted channel estimation. In further work, we will theoretically analyze the MMMC achieved with more general equidistant PAs to reveal the reason why this type of PA is unsuitable. Moreover, we will explore other low complexity PA methods to further reduce the difficulty of practical application.

ACKNOWLEDGMENT

This work is supported by a Belgian EOS grant with project grant number EOS30452698, the Flemish Fund for Scientific

Research (FWO) and the National Natural Science Foundation of China under grant 61701530 and 61801516.

REFERENCES

- [1] J. H. Reed, *Introduction to ultra wideband communication systems*. Prentice Hall Press, 2005.
- [2] J. L. Paredes, G. R. Arce, and Z. Wang, "Ultra-wideband compressed sensing: Channel estimation," *IEEE Journal of Selected Topics in Signal Processing*, vol. 1, no. 3, pp. 383–395, 2007.
- [3] M. Başaran, S. Erküçük, and H. A. Çırpan, "Compressive sensing for ultra-wideband channel estimation: on the sparsity assumption of ultra-wideband channels," *International Journal of Communication Systems*, vol. 27, no. 11, pp. 3383–3398, 2014.
- [4] E. J. Candès, J. Romberg, and T. Tao, "Robust uncertainty principles: Exact signal reconstruction from highly incomplete frequency information," *IEEE Transactions on Information Theory*, vol. 52, no. 2, pp. 489–509, 2006.
- [5] D. L. Donoho, "Compressed sensing," *IEEE Transactions on Information Theory*, vol. 52, no. 4, pp. 1289–1306, 2006.
- [6] E. Lagunas and M. Nájár, "Sparse channel estimation based on compressed sensing for ultra wideband systems," in *2011 IEEE international conference on ultra-wideband (ICUWB)*. IEEE, 2011, pp. 365–369.
- [7] Y. Zhang, R. Venkatesan, O. A. Dobre, and C. Li, "Novel compressed sensing-based channel estimation algorithm and near-optimal pilot placement scheme," *IEEE Transactions on Wireless Communications*, vol. 15, no. 4, pp. 2590–2603, 2015.
- [8] T. Yaacoub, O. A. Dobre, R. Youssef, and E. Radoi, "Optimal selection of fourier coefficients for compressed sensing-based uwb channel estimation," *IEEE Wireless Communications Letters*, vol. 6, no. 4, pp. 466–469, 2017.
- [9] D. L. Donoho, M. Elad, and V. N. Temlyakov, "Stable recovery of sparse overcomplete representations in the presence of noise," *IEEE Transactions on Information Theory*, vol. 52, no. 1, pp. 6–18, 2006.
- [10] X. He, R. Song, and W.-P. Zhu, "Optimal pilot pattern design for compressed sensing-based sparse channel estimation in OFDM systems," *Circuits, Systems, and Signal Processing*, vol. 31, no. 4, pp. 1379–1395, 2012.
- [11] P. Pakrooh, A. Amini, and F. Marvasti, "OFDM pilot allocation for sparse channel estimation," *EURASIP Journal on Advances in Signal Processing*, vol. 2012, no. 1, p. 59, 2012.
- [12] C. Qi, G. Yue, L. Wu, Y. Huang, and A. Nallanathan, "Pilot design schemes for sparse channel estimation in OFDM systems," *IEEE Transactions on Vehicular Technology*, vol. 64, no. 4, pp. 1493–1505, 2015.
- [13] C.-Y. Chen and P. Vaidyanathan, "Compressed sensing in MIMO radar," in *2008 42nd Asilomar Conference on Signals, Systems and Computers*. IEEE, 2008, pp. 41–44.
- [14] J. Wang, W.-X. Sheng, Y.-B. Han, and X.-F. Ma, "Adaptive beamforming with compressed sensing for sparse receiving array," *IEEE Transactions on Aerospace and Electronic Systems*, vol. 50, no. 2, pp. 823–833, 2014.
- [15] A. R. Bahai, B. R. Saltzberg, and M. Ergen, *Multi-carrier digital communications: theory and applications of OFDM*. Springer Science & Business Media, 2004.
- [16] S. Kirkpatrick, C. D. Gelatt, and M. P. Vecchi, "Optimization by simulated annealing," *science*, vol. 220, no. 4598, pp. 671–680, 1983.
- [17] M.-W. Park and Y.-D. Kim, "A systematic procedure for setting parameters in simulated annealing algorithms," *Computers & Operations Research*, vol. 25, no. 3, pp. 207–217, 1998.
- [18] D. Needell and J. A. Tropp, "CoSaMP: Iterative signal recovery from incomplete and inaccurate samples," *Applied and Computational Harmonic Analysis*, vol. 26, no. 3, pp. 301–321, 2009.
- [19] C. Ion, *Advances in Quantum Theory*. IntechOpen, 2012.
- [20] W. Dai and O. Milenkovic, "Subspace pursuit for compressive sensing signal reconstruction," *IEEE Transactions on Information Theory*, vol. 55, no. 5, pp. 2230–2249, 2009.
- [21] J. A. Tropp and A. C. Gilbert, "Signal recovery from random measurements via orthogonal matching pursuit," *IEEE Transactions on Information Theory*, vol. 53, no. 12, pp. 4655–4666, 2007.